PHOTONICS Research

Extraordinary characteristics for one-dimensional parity-time-symmetric periodic ring optical waveguide networks

Yan Zhi,[1] Xiangbo Yang,[1,2,3,*] Jiaye Wu,[2] Shiping Du,[4] Peichao Cao,[1] Dongmei Deng,[2] and Chengyi Timon Liu[3]

[1]MOE Key Laboratory of Laser Life Science and Institute of Laser Life Science, College of Biophotonics, South China Normal University, Guangzhou 510631, China
[2]Guangzhou Key Laboratory for Special Fiber Photonic Devices, School of Information and Optoelectronic Science and Engineering, South China Normal University, Guangzhou 510006, China
[3]School of Physical Education and Sports Science, South China Normal University, Guangzhou 510006, China
[4]Department of Data and Computer Science, Sun Yat-sen University, Guangzhou 510006, China
*Corresponding author: xbyang@scnu.edu.cn

Received 19 January 2018; revised 28 March 2018; accepted 29 March 2018; posted 30 March 2018 (Doc. ID 318894); published 23 May 2018

In this paper, we design a one-dimensional (1D) parity-time-symmetric periodic ring optical waveguide network (PTSPROWN) and investigate its extraordinary optical characteristics. It is found that quite different from traditional vacuum/dielectric optical waveguide networks, 1D PTSPROWN cannot produce a photonic ordinary propagation mode, but can generate simultaneously two kinds of photonic nonpropagation modes: attenuation propagation mode and gain propagation mode. It creates neither passband nor stopband and possesses no photonic band structure. This makes 1D PTSPROWN possess richer spontaneous PT-symmetric breaking points and causes interesting extremum spontaneous PT-symmetric breaking points to appear, where electromagnetic waves can create ultrastrong extraordinary transmission, reflection, and localization, and the maximum can arrive at 6.6556×10^{12} and is more than 7 orders of magnitude larger than the results reported previously. 1D PTSPROWN may possess potential in designing high-efficiency optical energy saver devices, optical amplifiers, optical switches with ultrahigh monochromaticity, and so on.

OCIS codes: (230.7370) Waveguides; (160.4670) Optical materials; (160.3918) Metamaterials.

https://doi.org/10.1364/PRJ.6.000579

1. INTRODUCTION

In the wake of photonic crystals and metamaterials, the parity-time-symmetric (PT-symmetric) optical system is another kind of new artificial structure to control and confine the propagation of electromagnetic (EM) waves. Since it was proposed in 2007 [1], people have paid great attention to it [1–17]. It is well known that eigenvalues of Hermitian operators in quantum mechanics are all real numbers, and the operators corresponding to observable mechanical quantities should be Hermitian ones in order to make their eigenvalues be real numbers. In 1998, Bender *et al.* [18,19] found that for a PT-symmetric dynamic system, when the imaginary part of the potential function is smaller than some critical value, even if its Hamiltonian operator is non-Hermitian, all the energy eigenvalues are still real numbers; only when the imaginary part of its potential function is larger than this critical value do its energy eigenvalues appear to be complex numbers. This critical value is called the spontaneous PT-symmetric breaking point. In 2007, El-Ganainy *et al.* [1] constructed PT-symmetric optical systems by materials with even-function real part and odd-function imaginary part refractive indices on the condition of paraxial approximation. Subsequently, people have widely investigated extraordinary optical features and phenomena in PT-symmetric optical systems, such as new solitons [2,7,8,11,12], Bloch oscillations [3,4], noncommutability [3,9], unidirectional invisibility [5,9,10,13,14], dual behavior of PT-symmetric scattering [3,10], 2×2 spatial optical switches [6], and ultrastrong transmission and reflection [9,15,16].

An optical waveguide network [20,21] is another kind of new remarkable artificial structure to control and confine the propagation of EM waves. Just like photonic crystals, an optical waveguide network has a kind of photonic bandgap (PBG) structure. Compared with the former, the structure symmetry of the latter is much more flexible [20,22,23], and the phase and amplitude measurements of the EM wave in the latter are also much more convenient [20,23]. It is found that optical

waveguide networks can produce rich photonic attenuation mode [24], interesting comb-like optical transmission spectrum [25,26], extreme wide PBG [22,27,28], ultrastrong photonic localization [29–32], and so on.

Optical waveguide networks now studied are mainly composed of dielectrics and/or materials with a single negative refractive index. Now it is known that PT-symmetric waveguides are quite different from the former and possess extraordinary optical characteristics, so, if the former is replaced by the latter, will the networks produce new photonic propagation modes and then generate new extraordinary optical characteristics? Investigations on these networks may deepen people's knowledge of PBG materials and PT-symmetric optical structures and may be helpful for controlling and confining the propagation of EM waves.

In this paper, we design a one-dimensional (1D) PT-symmetric periodic ring optical waveguide network (1D PTSPROWN) by use of magnesium fluoride (MgF_2) materials and investigate the propagation of EM waves in this network. It is found that, quite different from the PT-symmetric optical structures already reported, in our designed 1D PTSPROWN, a photonic ordinary propagation mode (OPM) cannot be generated; only two kinds of special nonpropagation modes can be produced, which can create new photonic mode distribution, extremum spontaneous PT-symmetric breaking points, and ultrastrong extraordinary photonic transmission, reflection, and photonic localization. Our numerical results show that for either left- or right-incident EM waves, the maximal photonic transmission, reflection, and localization can all arrive at 6.6556×10^{12}, which is 7 orders of magnitude larger than the previous results. This interesting structure may possess potential applications for the design of efficient photonic energy storage, extreme narrowband optical filters, optical amplifiers, optical logic elements in photon computers, and ultrasensitive optical switches with ultrahigh monochromaticity, etc. On the other hand, the structure of our designed 1D PTSPROWN is very simple, and the imaginary part of the refractive index of the waveguide material is very small. It may be realized conveniently in experiments.

This paper is organized as follows. In Section 2, we introduce our designed 1D PTSPROWN and the main theory and method for analytical deducing and numerical calculation. In Section 3, we deduce the general network equation for a three-material optical waveguide network. The analytical and numerical results of the extraordinary optical properties and the discussions on them are given in Section 4. Finally, Section 5 is the summary of this paper.

2. MODEL AND THEORY

A. 1D PTSPROWN

The 1D PTSPROWN studied in this paper is shown in Fig. 1, where the length for each waveguide segment is d. In order to compare the calculations with experimental results, in Subsection 4.B, we set the wavelength of the first extremum spontaneous PT-symmetric breaking point near the communication wavelength $\lambda = 1.550$ μm by adjusting the length parameter d. For this reason, in this paper we set $d = 11.3095$ μm. In Fig. 1, the thin black solid lines at the entrance and exit are all vacuum optical waveguide segments,

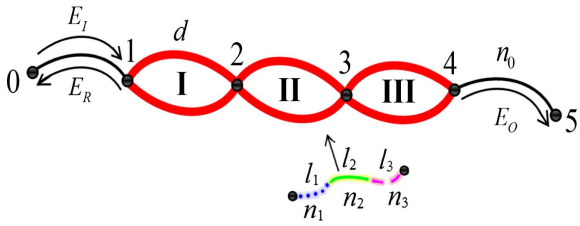

Fig. 1. Schematic of the 1D PTSPROWN, including three unit cells, one entrance, and one exit, where E_I, E_R, and E_O are the input, reflective, and output EM waves, respectively, and the length for each waveguide segment is d. The thin black solid lines at the entrance and exit are all vacuum optical waveguide segments. The thick red solid lines in unit cells are PT-symmetric optical waveguide segments, where the refractive indices of the three subwaveguides are, respectively, n_1, n_2, and n_3, and their length ratios are l_1, l_2, and l_3, respectively.

and the refractive index is $n_0 = 1$. The thick red solid lines in unit cells are PT-symmetric optical waveguide segments that are made of MgF_2, and their complex conjugate refractive indices along the length can be realized in two ways: doping gain and loss quantum dots [15], or modulating the density of materials [32]. The refractive indices of the three subwaveguides are, respectively,

$$\begin{cases} n_1 = n_{MgF_2} - \imath n_b, \\ n_2 = n_{MgF_2}, \\ n_3 = n_{MgF_2} + \imath n_b, \end{cases} \tag{1}$$

and their length ratios are $l_1 = l_2 = l_3 = \frac{1}{3}$.

For MgF_2, it is reported that in the range of 43–1500 THz (i.e., 0.20–7.00 μm), the dispersion equation satisfies [33]

$$n^2_{MgF_2} - 1 = \frac{0.48755108\lambda^2}{\lambda^2 - 0.04338408^2} + \frac{0.39875031\lambda^2}{\lambda^2 - 0.09461442^2} + \frac{2.312035\lambda^2}{\lambda^2 - 23.793604^2}, \tag{2}$$

and the dispersion curve is plotted in Fig. 2.

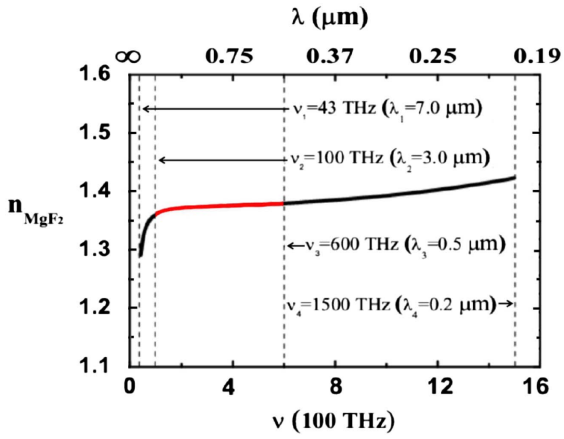

Fig. 2. Dispersion curve of MgF_2 defined by Eq. (2), where the thick red solid line expresses the range investigated in this paper; the thin black dashed lines are all scaling lines, and the values are, respectively, $\nu_1 = 43$ THz ($\lambda_1 = 7.00$ μm), $\nu_2 = 100$ THz ($\lambda_2 = 3.0$ μm), $\nu_3 = 600$ THz ($\lambda_3 = 0.5$ μm), and $\nu_4 = 1500$ THz ($\lambda_4 = 0.2$ μm).

From Fig. 2, one can see that in the range of 100–1500 THz (i.e., 0.2–3.0 μm), the dispersion effect is weak. In order to reduce workload and the influence of dispersion effect on results, and at the same time in order to investigate the photonic properties near the communication wavelength, only the EM waves with the frequency (wavelength) in the range of 100–600 THz (0.5–3.0 μm) are studied, which corresponds to the dispersion curve of the thick red solid line in Fig. 2.

B. Generalized Floquet–Bloch Theorem

It is well known that the Floquet–Bloch theorem is used for investigating lattice waves in a system with spatial translation periodicity. However, in our designed optical waveguide network, all the waveguide segments can be arbitrarily bent and folded, and consequently, only topological translation periodicity, but no spatial translation periodicity, exists. For this kind of structure, recently we proposed a dimensionless generalized Floquet–Bloch theorem [23], which can be expressed as

$$\psi_{\vec{K}}(\vec{N}+\vec{T})=\psi_{\vec{K}}(\vec{N})e^{\imath\vec{K}\cdot\vec{T}}, \tag{3}$$

where $\vec{K}$ is the structure Bloch wave vector, $\vec{N}$ is the node scaling vector, and $\vec{T}$ is the structure translation vector. In this paper, we use the generalized Floquet–Bloch theorem to deduce dispersion relation, define photonic modes, and determine the distribution of photonic modes.

C. Generalized Eigenfunction Method

In this paper, we use the generalized eigenfunction method [34] to calculate transmissivity, reflectivity, and photonic localization, where wave transfer equations are changed into a transfer matrix, and transmission and reflection coefficients are regarded as generalized wave functions.

3. THREE-MATERIAL NETWORK EQUATION

In the 1D PTSPROWN shown in Fig. 1, optical waveguides in unit cells are PT-symmetric waveguide segments and are made up of three kinds of materials. So, the reported one-material network equation [23,35] and two-material network equation [26] are not suitable. In this section, we deduce a three-material network equation.

In a three-material network, EM waves satisfy the following wave equation [35]:

$$\frac{\partial^2}{\partial x^2}\psi_{n_m}(x)+k_m^2\psi_{n_m}(x)=0, \tag{4}$$

where the wave vector $k_m=2\pi\nu n_m/c$ $(m=1,2,3)$, ν is the EM wave frequency, and $c=2.99792458\times10^8$ m/s is the speed of EM waves in vacuum.

For 1D waveguide segments, only the monomode propagation of EM waves needs to be considered. The wave function between nodes i and j can be regarded as the following linear combination of two opposite traveling plane waves:

$$\psi_{ij}(x)=\begin{cases}\psi_{n_1}(x)=a_1e^{\imath k_1x}+b_1e^{-\imath k_1x}\\ \qquad(0\le x\le l_1d_{ij}),\\ \psi_{n_2}(x)=a_2e^{\imath k_2x}+b_2e^{-\imath k_2x}\\ \qquad(l_1d_{ij}\le x\le l_{12}d_{ij}),\\ \psi_{n_3}(x)=a_3e^{\imath k_3x}+b_3e^{-\imath k_3x}\\ \qquad(l_{12}d_{ij}\le x\le d_{ij}),\end{cases} \tag{5}$$

where $l_{12}=l_1+l_2$. At the sites of $x=l_1d_{ij}$ and $l_{12}d_{ij}$, by means of the continuities of the wave function and its differential quotient, one can obtain that

$$\begin{cases}a_1e^{\imath k_1l_1d_{ij}}+b_1e^{-\imath k_1l_1d_{ij}}\\ \qquad=a_2e^{\imath k_2l_1d_{ij}}+b_2e^{-\imath k_2l_1d_{ij}},\\ a_1k_1e^{\imath k_1l_1d_{ij}}-b_1k_1e^{-\imath k_1l_1d_{ij}}\\ \qquad=a_2k_2e^{\imath k_2l_1d_{ij}}-b_2k_2e^{-\imath k_2l_1d_{ij}},\\ a_3e^{\imath k_3l_{12}d_{ij}}+b_3e^{-\imath k_3l_{12}d_{ij}}\\ \qquad=a_2e^{\imath k_2l_{12}d_{ij}}+b_2e^{-\imath k_2l_{12}d_{ij}},\\ a_3k_3e^{\imath k_3l_{12}d_{ij}}-b_3k_3e^{-\imath k_3l_{12}d_{ij}}\\ \qquad=a_2k_2e^{\imath k_2l_{12}d_{ij}}-b_2k_2e^{-\imath k_2l_{12}d_{ij}}.\end{cases} \tag{6}$$

By use of Eqs. (5) and (6), one can deduce that

$$\psi_{ij}(x)=\begin{cases}\psi_{n_1}(x)=\frac{\Omega_1e^{\imath\Pi_1}+\Omega_2e^{\imath\Pi_2}}{2k_1}a_2\\ \qquad+\frac{\Omega_1e^{-\imath\Pi_1}+\Omega_2e^{-\imath\Pi_2}}{2k_1}b_2\\ \qquad(0\le x\le l_1d_{ij}),\\ \psi_{n_2}(x)=a_2e^{\imath k_2x}+b_2e^{-\imath k_2x}\\ \qquad(l_1d_{ij}\le x\le l_{12}d_{ij}),\\ \psi_{n_3}(x)=\frac{\Xi_1e^{\imath\Theta_1}+\Xi_2e^{\imath\Theta_2}}{2k_3}a_2\\ \qquad+\frac{\Xi_1e^{-\imath\Theta_1}+\Xi_2e^{-\imath\Theta_2}}{2k_3}b_2\\ \qquad(l_{12}d_{ij}\le x\le d_{ij}),\end{cases} \tag{7}$$

where

$$\begin{cases}\Omega_1=k_1+k_2,\\ \Omega_2=k_1-k_2,\\ \Pi_1=k_2l_1d_{ij}-k_1l_1d_{ij}+k_1x,\\ \Pi_2=k_2l_1d_{ij}+k_1l_1d_{ij}-k_1x,\\ \Xi_1=k_3+k_2,\\ \Xi_2=k_3-k_2,\\ \Theta_1=k_2l_{12}d_{ij}-k_3l_{12}d_{ij}+k_3x,\\ \Theta_2=k_2l_{12}d_{ij}+k_3l_{12}d_{ij}-k_3x.\end{cases} \tag{8}$$

If ψ_i and ψ_j denote the wave functions at nodes i and j, respectively, by use of the continuity of the wave functions, one can obtain that

$$\begin{cases}\psi_{ij}(x)|_{x=0}=\psi_i,\\ \psi_{ij}(x)|_{x=d_{ij}}=\psi_j.\end{cases} \tag{9}$$

By means of Eqs. (7)–(9), one can obtain that

$$\begin{cases}\frac{\Omega_1e^{\imath\Upsilon_2}+\Omega_2e^{\imath\Upsilon_1}}{2k_1}a_2+\frac{\Omega_1e^{-\imath\Upsilon_2}+\Omega_2e^{-\imath\Upsilon_1}}{2k_1}b_2=\psi_i,\\ \frac{\Xi_1e^{\imath\Upsilon_4}+\Xi_2e^{\imath\Upsilon_3}}{2k_3}a_2+\frac{\Xi_1e^{-\imath\Upsilon_4}+\Xi_2e^{-\imath\Upsilon_3}}{2k_3}b_2=\psi_j,\end{cases} \tag{10}$$

where

$$\begin{cases}\Upsilon_1=k_2l_1d_{ij}+k_1l_1d_{ij},\\ \Upsilon_2=k_2l_1d_{ij}-k_1l_1d_{ij},\\ \Upsilon_3=k_2l_{12}d_{ij}-k_3l_3d_{ij},\\ \Upsilon_4=k_2l_{12}d_{ij}+k_3l_3d_{ij}.\end{cases} \tag{11}$$

By means of Eqs. (7), (8), (10), and (11), one can obtain that

$$\psi_{n_1}(x) = \psi_i\xi_1\frac{\Omega_1\cos(\Upsilon_2 + k_1x) + \Omega_2\cos(\Upsilon_1 - k_1x)}{\sum_{\alpha,\beta}\Omega_\alpha\Xi_\beta(-1)^{\alpha+\beta}\sin d_{ij}Z_{\alpha,\beta}} - \psi_i\xi_2\frac{\Omega_1\sin(\Upsilon_2 + k_1x) + \Omega_2\sin(\Upsilon_1 - k_1x)}{\sum_{\alpha,\beta}\Omega_\alpha\Xi_\beta(-1)^{\alpha+\beta}\sin d_{ij}Z_{\alpha,\beta}} - \frac{k_3}{k_1}\psi_j\xi_3\frac{\Omega_1\cos(\Upsilon_2 + k_1x) + \Omega_2\cos(\Upsilon_1 - k_1x)}{\sum_{\alpha,\beta}\Omega_\alpha\Xi_\beta(-1)^{\alpha+\beta}\sin d_{ij}Z_{\alpha,\beta}} + \frac{k_3}{k_1}\psi_j\xi_4\frac{\Omega_1\sin(\Upsilon_2 + k_1x) + \Omega_2\sin(\Upsilon_1 - k_1x)}{\sum_{\alpha,\beta}\Omega_\alpha\Xi_\beta(-1)^{\alpha+\beta}\sin d_{ij}Z_{\alpha,\beta}}, \tag{12}$$

where

$$\begin{cases} \alpha,\beta = 1,2, \\ Z_{1,1} = k_1l_1 + k_2l_2 + k_3l_3, \\ Z_{2,1} = k_1l_1 - k_2l_2 - k_3l_3, \\ Z_{1,2} = k_1l_1 + k_2l_2 - k_3l_3, \\ Z_{2,2} = k_1l_1 - k_2l_2 + k_3l_3, \\ \xi_1 = \Xi_2\sin\Upsilon_3 + \Xi_1\sin\Upsilon_4, \\ \xi_2 = \Xi_2\cos\Upsilon_3 + \Xi_1\cos\Upsilon_4, \\ \xi_3 = \Omega_2\sin\Upsilon_1 + \Omega_1\sin\Upsilon_2, \\ \xi_4 = \Omega_1\cos\Upsilon_2 + \Omega_2\cos\Upsilon_1. \end{cases} \tag{13}$$

At any node, the energy flux conservation gives

$$\sum_j \frac{1}{\mu\omega}A_{ij}\psi_{ij}(x)\frac{\partial\psi_{ij}(x)}{\partial x}\bigg|_{x=0} = 0, \tag{14}$$

where the summation is over all segments linked directly to node i. Generally, the cross-sectional area A_{ij} for each segment is the same; the boundary conditions, Eqs. (9) and (14), yield

$$\sum_j \frac{\partial\psi_{ij}(x)}{\partial x}\bigg|_{x=0} = 0. \tag{15}$$

In order to obtain the relationship between the wave functions of nearest-neighbor nodes in the network systems, one can deduce the following network equation of the three-material multiconnected network by putting Eqs. (7), (8), (12), and (13) into Eq. (15):

$$-\psi_i\sum_j\frac{\sum_{\alpha,\beta}\Omega_\alpha\Xi_\beta(-1)^{\alpha+\beta}\cos d_{ij}Z_{\alpha,\beta}}{\sum_{\alpha,\beta}\Omega_\alpha\Xi_\beta(-1)^{\alpha+\beta}\sin d_{ij}Z_{\alpha,\beta}} + \sum_j\psi_j\frac{4k_2k_3}{\sum_{\alpha,\beta}\Omega_\alpha\Xi_\beta(-1)^{\alpha+\beta}\sin d_{ij}Z_{\alpha,\beta}} = 0. \tag{16}$$

In order to test the correctness of the three-material multiconnected network equation, we compare Eq. (16) with the reported one-material network equation [35], the vacuum optical waveguide network equation [23], and the two-material network equation [26]. When $n_1 \neq n_2$ and $n_2 = n_3$, the three-material network degenerates to a two-material system, and Eq. (16) changes into

$$-\psi_i\sum_j\frac{\Omega_1\cos d_{ij}Z_{11} - \Omega_2\cos d_{ij}Z_{21}}{\Omega_1\sin d_{ij}Z_{11} - \Omega_2\sin d_{ij}Z_{21}} + \sum_j\psi_j\frac{2k_2}{\Omega_1\sin d_{ij}Z_{11} - \Omega_2\sin d_{ij}Z_{21}} = 0. \tag{17}$$

Obviously, when

$$\begin{cases} \Omega_1 = \Phi, \\ \Omega_2 = -\Gamma, \\ d_{ij}Z_{11} = \Pi + \Theta, \\ d_{ij}Z_{21} = \Pi - \Theta, \end{cases} \tag{18}$$

our deduced two-material waveguide network equation, Eq. (17), is exactly accordant with the reported one [26]. When $n_1 = n_2 = n_3$, the three-material network degenerates to a one-material system, and Eq. (16) changes into

$$-\psi_i\sum_j\cot kd_{ij} + \sum_j\psi_j\csc kd_{ij} = 0, \tag{19}$$

where $k = 2\pi\nu n/c$. Obviously, when

$$\begin{cases} d_{ij} = l_{ij}, \\ k = -\imath Z, \end{cases} \tag{20}$$

our deduced one-material waveguide network equation, Eq. (19), is exactly accordant with the reported one [35]. In this paper, we use the three-material multiconnected network equation, Eq. (16), to investigate the extraordinary optical characteristics of PT-symmetric optical waveguide networks.

4. EXTRAORDINARY OPTICAL PROPERTIES

A. Extraordinary Photonic Modes

From the generalized Floquet–Bloch theorem, one knows that when EM waves propagate in the optical waveguide network with topological translation periodicity, the only difference between the wave function in the Nth unit cell and that in the $(N+T)$th unit cell is a phase factor of $e^{\imath\vec{K}\cdot\vec{T}}$. When the structure Bloch wave vector K is a real number, $\vec{K}\cdot\vec{T}$ is also a real number. When EM waves propagate in this kind of network, the amplitude of the wave function keeps constant, though the phase of the wave function changes with a factor, $e^{\imath\vec{K}\cdot\vec{T}}$. We call this kind of photonic mode OPM [24]. When $K = K_a + \imath K_b$ $(K_b > 0)$ is a complex number, $\imath\vec{K}\cdot\vec{T} = -K_bT + \imath K_aT$. When EM waves propagate in this kind of network, not only the phase of the wave function changes with a factor, $e^{\imath K_aT}$, but also the amplitude of the wave function attenuates with a factor, e^{-K_bT}. We call this kind of photonic mode attenuation propagation mode (APM), which is one of the nonpropagation modes. When $K = K_a - \imath K_b$ $(K_b > 0)$ is a complex number, $\imath\vec{K}\cdot\vec{T} = K_bT + \imath K_aT$. When EM waves propagate in this kind of network, not only the phase of the wave function changes with a factor, $e^{\imath K_aT}$, but also the amplitude of the wave function gains with a factor, e^{K_bT}. We call this kind of photonic mode gain propagation mode (GPM), which is also one of the nonpropagation modes.

For 1D PTSPROWNs with infinite unit cells, based on the generalized Floquet–Bloch theorem and the three-material network equation, one can deduce the following dispersion relation:

$$\cos K = f(\nu), \tag{21}$$

where

$$f(\nu) = \sum_{ij} \frac{\sum_{\alpha,\beta} \Omega_\alpha \Xi_\beta (-1)^{\alpha+\beta} \cos d_{ij} Z_{\alpha,\beta}}{\sum_{\alpha,\beta} \Omega_\alpha \Xi_\beta (-1)^{\alpha+\beta} \sin d_{ij} Z_{\alpha,\beta}} + \sum_{ij} \frac{4k_2 k_3}{\sum_{\alpha,\beta} \Omega_\alpha \Xi_\beta (-1)^{\alpha+\beta} \sin d_{ij} Z_{\alpha,\beta}}, \tag{22}$$

and $\alpha, \beta = 1,2$.

For 1D three-material ring optical waveguide networks composed of vacuum and/or dielectric waveguides, where the material refractive indices are all real, it is known from Eq. (22) that the dispersion function $f(\nu)$ must be real. For real $f(\nu)$ and $|f(\nu)| \le 1$, from Eq. (21) one can deduce that the structure Bloch wave vector K possesses real solutions, and EM waves in this frequency range propagate as OPM and form passbands. Consequently, large transmission is produced, and the transmissivity does not decrease with the increasing number of unit cells and generally satisfies $0.01 \le T \le 1.0$. However, for real $f(\nu)$ and $|f(\nu)| > 1$, from Eq. (21) one can deduce that the structure Bloch wave vector K possesses a pair of complex conjugate solutions. From the aspect of mathematics, EM waves in this frequency range will propagate as APM and GPM simultaneously, but in the optical waveguide networks composed of vacuum and/or dielectric waveguides, there exists only an attenuation mechanism but no gain mechanism, and consequently, from the aspect of physics, EM waves in this frequency range will propagate only as APM and form stopbands. Then very small transmission is produced, and the transmissivity decreases with the increasing number of unit cells and generally satisfies $T < 0.01$. It shows that in the optical waveguide networks composed of vacuum and/or dielectric waveguides, $|f(\nu)| = 1$ is a critical point for adjusting photonic modes.

For our designed 1D PTSPROWN, where the refractive indices of two kinds of materials are complex, one can deduce from Eq. (22) that the dispersion function $f(\nu)$ keeps being complex in the total range of frequency. For complex $f(\nu)$, from Eq. (21) one can see that the structure Bloch wave vector K possesses no real solution, but a pair of complex conjugate ones. From the aspect of mathematics, EM waves in this PT-symmetric network will propagate as APM and GPM simultaneously. On the other hand, in PT-symmetric optical waveguides, both attenuation and gain mechanisms exist, and consequently, from the aspect of physics, EM waves will propagate as APM and GPM simultaneously. It means that in this PT-symmetric network the structure Bloch wave vector K possesses no real solution but a pair of complex conjugate ones, and then no matter whether the transmissivity decreases with the increasing number of unit cells and whichever range the EM wave frequency is, the traditional passbands and/or stopbands will not exist now.

In short, the photonic modes in PT-symmetric optical waveguide networks are quite different from those in vacuum and/or dielectric optical waveguide networks. For the former, no OPM exists, but APM and GPM exist simultaneously in the total range of frequency; for the latter, no GPM in the total range of frequency exists, but OPM and APM in some other frequency range(s) exist. For the former, no passband and/or stopband is formed, and then no traditional band structure exists; for the latter, passband and/or stopband can be formed, and then a traditional band structure exists. The former can produce extraordinary transmission, where transmissivity is much larger than 1.0, but the latter can only generate ordinary transmission, where transmissivity is equal to or smaller than 1.0.

Additionally, it has been reported that spontaneous PT-symmetric breaking points are located at the boundary between the photonic OPM and nonpropagation modes [1–3,7–10,36]. However, when EM waves propagate in our designed 1D PTSPROWN, no OPM exists except two kinds of nonpropagation modes, APM and GPM, simultaneously, in the total range of frequency, and they cannot be separated from each other anywhere and anytime. Consequently, spontaneous PT-symmetric breaking points of our designed 1D PTSPROWN cannot be determined by photonic APM and GPM. From Eq. (21), one can see that when the absolute value of dispersion function $|f(\nu)|$ is small, the imaginary part of the structure Bloch wave vector K may also be small, and extraordinary transmissivity with the value larger than 1.0 cannot be created. Only when $|f(\nu)|$ is big enough can the imaginary part of K be very large and the extraordinary transmissivity with the value larger than 1.0 be generated. For this reason, just as with vacuum and/or dielectric waveguide networks, we choose $|f(\nu)| = 1$ to be the critical value for adjusting photonic modes, define both APM and GPM produced by the PT-symmetric waveguide network corresponding to $|f(\nu)| \le 1$ as weak propagation modes (WPMs), and define those produced by the PT-symmetric waveguide network corresponding to $|f(\nu)| > 1$ as strong propagation modes (SPMs). On this condition, we define the spontaneous PT-symmetric breaking points of our designed 1D PTSPROWN as the imaginary part of the PT-symmetric materials, n_b, located between WPM and SPM.

B. Extremum Spontaneous PT-Symmetric Breaking Points

According to the definitions in Subsection 4.A for photonic WPM and SPM and spontaneous PT-symmetric breaking points in 1D PTSPROWN, by using Eq. (22), we plot in Fig. 3 the distribution diagram of photonic modes for the EM waves in the range of 100–600 THz (0.5–3.0 μm).

From Fig. 3, one can see that five extremum valleys for the spontaneous PT-symmetric breaking points of 1D PTSPROWN exist. We call them extremum spontaneous PT-symmetric breaking points, whose data are

$$\begin{cases} \nu_{\mathrm{I}} = 193.4158\ \mathrm{THz}, & n_{\mathrm{bcosI}} = 2.181 \times 10^{-8}; \\ \nu_{\mathrm{II}} = 289.5226\ \mathrm{THz}, & n_{\mathrm{bcosII}} = 2.776 \times 10^{-6}; \\ \nu_{\mathrm{III}} = 385.4978\ \mathrm{THz}, & n_{\mathrm{bcosIII}} = 2.190 \times 10^{-8}; \\ \nu_{\mathrm{IV}} = 481.2158\ \mathrm{THz}, & n_{\mathrm{bcosIV}} = 2.462 \times 10^{-8}; \\ \nu_{\mathrm{V}} = 576.5832\ \mathrm{THz}, & n_{\mathrm{bcosV}} = 4.562 \times 10^{-6}. \end{cases} \tag{23}$$

At these extremum points, $|f(\nu)| = 1$ exists, and the dispersion function $f(\nu)$ is continuous without derivative. It makes photons create ultrastrong extraordinary transmission and reflection.

C. Extraordinary Transmission and Reflection

In order to investigate the properties of transmission and reflection of 1D PTSPROWN, we numerically calculate the

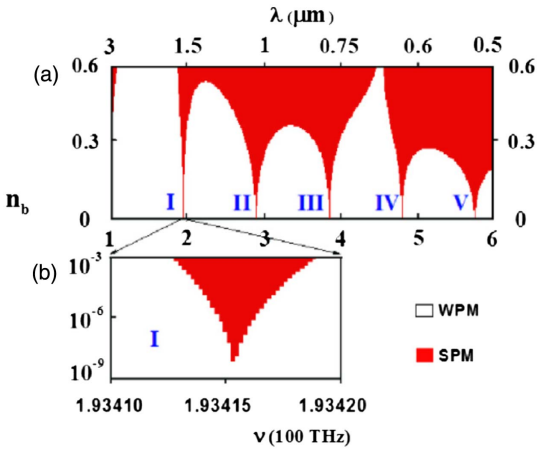

Fig. 3. Distribution diagram of photonic modes, where white and red zones represent WPMs and SPMs, respectively. (a) Frequency range corresponds to the thick red solid line in Fig. 2. (b) Enlarged drawing of the zone for the first extremum spontaneous PT-symmetric breaking point, whose location is near the communication wavelength, $\lambda = 1550$ nm.

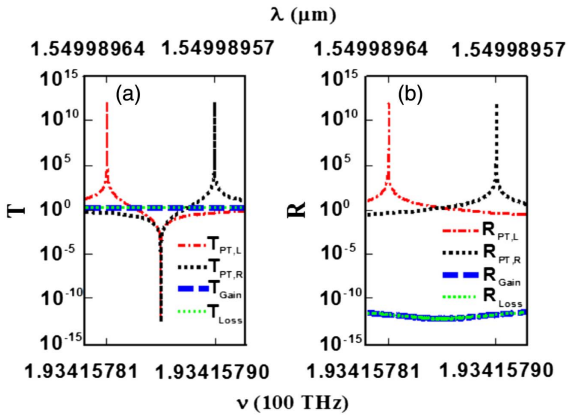

Fig. 4. Transmission and reflection spectra at the first extremum spontaneous PT-symmetric breaking point of the 1D ring optical waveguide network with three unit cells, where red dashed and dotted lines and black dotted lines express left- and right-incident results of PT-symmetric network, respectively; thick blue dashed lines denote the results of pure gain-material network with the refractive index $n = 1.3705 - \imath 2.181 \times 10^{-8}$; thin green dotted lines indicate the results of pure loss-material network with the refractive index $n = 1.3705 + \imath 2.181 \times 10^{-8}$. (a) Transmission spectra; (b) reflection spectra.

transmissivity and reflectivity in the total frequency range of Fig. 3. It is found that the transmissivity and reflectivity in the pure white zone (WPM) or pure red zone (SPM) are generally smaller than those at the spontaneous PT-symmetric breaking points; the former is usually smaller than 1.0, while the latter is always bigger than 1.0. The transmissivity and reflectivity at the spontaneous PT-symmetric breaking points are much smaller than those at the extremum spontaneous PT-symmetric breaking points; the former is generally smaller than 10^5, while the latter's maximum can arrive at 10^{12}.

As an example, in Fig. 4 we plot the ultrastrong extraordinary transmission and reflection at the first extremum spontaneous PT-symmetric breaking point of the 1D PTSPROWN with three unit cells, where red dashed and dotted lines and black dotted lines express left- and right-incident results, respectively.

From Fig. 4, one can see that for 1D PTSPROWN, (i) at the points of $\nu = 193.415781$ THz and $\nu = 193.415790$ THz, for both left- and right-incident EM waves, and for both transmissivity and reflectivity, the maximums can all arrive at 6.6556×10^{12}, which is 7 orders of magnitude larger than the previous results; obviously, the 1D PTSPROWN shows ultrastrong extraordinary transmission and reflection; (ii) at the point of $\nu = 193.415786$ THz, for both left- and right-incident EM waves, the minimal transmissivity can arrive at 6.6556×10^{-12}; it means the 1D PTSPROWN shows an ultrastrong PBG-like attenuation characteristic; (iii) for both transmission and reflection spectra, the left-incident curves do not coincide with the right-incident ones; the 1D PTSPROWN shows typical noncommutability of EM wave propagation.

Why can 1D PTSPROWN produce ultrastrong extraordinary transmission and reflection? We think it is caused by the extraordinary photonic modes and the coupling resonant effect of gain and loss in this network. (i) First, it is known from the analyses on the photonic modes in Subsection 4.A that in 1D PTSPROWN, no OPM exists where the amplitude of the wave function keeps constant with the increasing number of unit cells, but two nonpropagation modes, APM and GPM, exist simultaneously in the total range of frequency, where the amplitude of the wave function attenuates and gains, respectively, with the increasing number of unit cells. These two kinds of nonpropagation modes are different not only from the OPM, but also from the nonpropagation modes produced by dielectric waveguide networks. When they propagate in the 1D PTSPROWN, neither passband nor stopband can be formed, and consequently, the transmission and reflection spectra for the 1D PTSPROWN are completely different from those of dielectric waveguide networks. (ii) On the other hand, in order to study the coupling resonant effect of gain and loss in PT-symmetric networks, we change the 1D PTSPROWN into 1D ring optical waveguide networks composed of single-gain and loss materials, respectively, and calculate their transmissivity and reflectivity. In order to compare the results conveniently with that of 1D PTSPROWN, we set the gain and loss materials in these two networks to just be the materials of the gain and loss unit cells of 1D PTSPROWN, i.e., at the communication wavelength $n_{\text{Gain}} = n_1 = 1.3705 - 2.181 \times 10^{-8}\imath$ and $n_{\text{Loss}} = n_3 = 1.3705 + 2.181 \times 10^{-8}\imath$. From Fig. 4(a), one can see that the transmissivity of the 1D ring optical waveguide network composed of single-gain material (the thick blue dashed line) is approximately 1.0001, and that of the 1D ring optical waveguide network composed of single-loss material (the thin green dotted line) is approximately 0.9998. It means that the transmissivity of the gain optical waveguide network is larger than 1.0, which is indeed bigger than that of the dielectric optical waveguide network, and is also extraordinary, but it is much smaller than that of the maximum of 1D PTSPROWN, where the latter arrives at the order of 10^{12}. Similarly, the transmissivity of the loss optical waveguide network is smaller than 1.0, but its

attenuation amplitude is much bigger than that of the minimum of 1D PTSPROWN, where the latter arrives at the order of 10^{-12}. The reason is that in the 1D ring optical waveguide network composed of single-gain/loss material, there only exists single-gain/loss mechanism/effect but no coupling mechanism/effect of gain and loss, and furthermore, we set the imaginary part of the gain/loss material be very small (only 10^{-8} order), so the single gain/loss effect is very weak. This means that in PT-symmetric networks, the pure gain and loss effects of both gain and loss materials on photons are all negligible and play subordinate roles; they will neither cancel nor weaken each other, but both couple and strengthen each other. The coupling of gain and loss effects plays a primary role. The gain and loss materials in each waveguide form a coupling resonant cavity and create a strong coupling resonant effect on the photons of APM and GPM and then produce sharp resonant peak and valley, whose resonant frequencies are determined by the network structure. On the other hand, we observe that the system response is nonreciprocal; the mechanism behind this nonreciprocity is still under investigation [37]. Because of the noncommutability of EM wave propagation, the resonant peaks for left and right incidence do not coincide with each other. (iii) Finally, compared with reported PT-symmetric optical structures, photons propagating in our designed 1D PTSPROWN will produce multiquantum coherent superposition; it strengthens the aforementioned coupling resonant effect. Based on this property, one can set the imaginary part of the PT-symmetric material to be very small. It will be convenient for the design of experiments and may decrease manufacturing costs.

D. Ultrastrong Photonic Localization

By means of generalized eigenfunction method [34] and Eq. (5), we numerically calculate the intensity distribution of photons in the 1D PTSPROWN. It is found that just as transmissivity and reflectivity, photonic localizations in the pure white zone (WPM) or pure red zone (SPM) are generally smaller than those at the boundaries between white and red zones (the spontaneous PT-symmetric breaking points); the former is usually smaller than 1.0, while the latter is always bigger than 1.0. The photonic localizations at the spontaneous PT-symmetric breaking points are much smaller than those at the extremum spontaneous PT-symmetric breaking points; the former is generally smaller than 10^5, while the latter's maximum can arrive at 10^{12}.

As an example, in Fig. 5 we plot the intensity map of the photonic localization at the first extremum spontaneous PT-symmetric breaking point of the 1D PTSPROWN with three unit cells. The upper arm is symmetric to the lower arm in each unit cell; the intensity distribution of EM waves in the former is also all the same as that in the latter. In order to avoid repetition, i–d–j ($i,j = 1,2,3$) in Fig. 5 expresses the upper or lower arm waveguide segment between nodes i and j.

From Fig. 5, one can see that the intensity distributions in the three unit cells are very similar to each other. At the resonant peak frequency, $\nu = 193.415781$ THz, in the upper or lower arm of each unit cell, EM waves create ultrastrong photonic localizations at the center and the two terminals, respectively, and the maximal intensities are all 6.6556×10^{12}. We think it is also caused by the extraordinary photonic modes

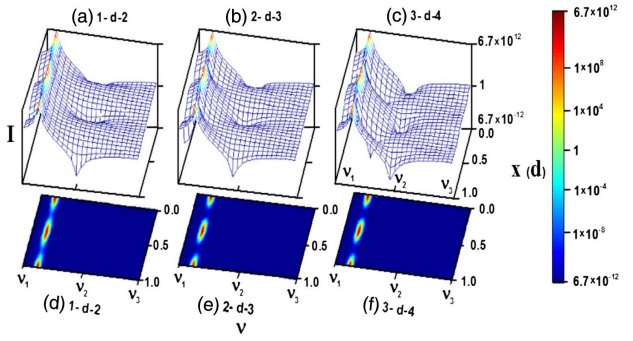

Fig. 5. Intensity map of the photonic localization at the first extremum spontaneous PT-symmetric breaking point of the 1D PTSPROWN with three unit cells, where i–d–j ($i,j = 1,2,3$) expresses the upper or lower arm waveguide segment between nodes i and j, and three frequencies are, respectively, $\nu_1 = 193.415780$ THz, $\nu_2 = 193.415787$ THz, and $\nu_3 = 193.415793$ THz. (a)–(c) Three-dimensional map; (d)–(f) two-dimensional map.

and the coupling resonant effect of gain and loss in this network. Each waveguide segment is a coupling resonant cavity, where EM waves form a standing-wave-like pattern.

Similarly, in Figs. 5(a)–5(c), at the resonant valley frequency, $\nu = 193.415786$ THz, in the upper or lower arm of each unit cell, EM waves create ultraweak photonic localizations at the center and the two terminals, respectively, and the minimal intensities are all 6.6556×10^{-12}. Coupling resonant effect of gain and loss causes EM waves to form a standing-wave-like pattern. The ultrastrong photonic localization indicates that 1D PTSPROWN may possess potential applications to the design of efficient photonic energy storage [26,27], ultrasensitive optical switches [28], and high power superluminescence diodes [29,30], and so on.

5. SUMMARY

In this paper, by use of the common material, MgF_2, we design an interesting 1D PTSPROWN and investigate the extraordinary optical characteristics when EM waves propagate in this network.

First of all, we obtain the network equation of the general three-material optical waveguide network and then deeply investigate the photonic modes in 1D PTSPROWN based on this network equation and the generalized Floquet–Bloch theorem. It is found that 1D PTSPROWN is quite different from vacuum and/or dielectric optical waveguide networks. (i) For the former, no OPM exists, but APM and GPM exist simultaneously in the total range of frequency; for the latter, no GPM in the total range of frequency exists, but OPM exists in some frequency range(s) and APM exists in some other frequency range(s). (ii) For the former, no passband and/or stopband is formed, and then no traditional band structure exists; for the latter, passband and/or stopband can be formed, and then a traditional band structure exists.

Based on these properties, we resort to photonic APM and GPM as WPM and SPM and define a new spontaneous PT-symmetric breaking point, which is different from those reported previously. We find that much richer spontaneous

PT-symmetric breaking points exist in our designed 1D PTSPROWN; even extremum PT-symmetric breaking points appear, where EM waves can generate extraordinary ultrastrong transmission, reflection, and localization, and the values are 7 orders of magnitude larger than the previous results. We think it is caused by the extraordinary photonic modes and the coupling resonant effect of gain and loss in this network. Each waveguide segment can be regarded as a coupling resonant cavity, where EM waves form a standing-wave-like pattern at the frequency of either the resonant peak or resonant valley. These interesting characteristics indicate 1D PTSPROWN may possess potential applications to the design of all-optical devices, such as efficient photonic energy storage, optical switches, and high-power superluminescence diodes [29,30].

Funding. National Natural Science Foundation of China (NSFC) (11674107, 11775083, 61475049, 61771205, 61774062); Natural Science Foundation of Guangdong Province (2015A030313374); Scientific Research Foundation of Graduate School of South China Normal University (2015lkxm27, 2017lkxm091).

REFERENCES

1. R. El-Ganainy, K. G. Makris, D. N. Christodoulides, and Z. H. Musslimani, "Theory of coupled optical PT-symmetric structures," Opt. Lett. **32**, 2632–2634 (2007).
2. Z. H. Musslimani, K. G. Makris, R. El-Ganainy, and D. N. Christodoulides, "Optical solitons in PT periodic potentials," Phys. Rev. Lett. **100**, 030402 (2008).
3. K. G. Makris, R. El-Ganainy, D. N. Christodoulides, and Z. H. Musslimani, "Beam dynamics in PT symmetric optical lattices," Phys. Rev. Lett. **100**, 103904 (2008).
4. S. Longhi, "Bloch oscillations in complex crystals with PT symmetry," Phys. Rev. Lett. **103**, 123601 (2009).
5. Z. Lin, H. Ramezani, T. Eichelkraut, T. Kottos, H. Cao, and D. N. Christodoulides, "Unidirectional invisibility induced by PT-symmetric periodic structures," Phys. Rev. Lett. **106**, 213901 (2011).
6. F. Nazari, M. Nazari, and M. K. Moravvej-Farshi, "A 2 × 2 spatial optical switch based on PT-symmetry," Opt. Lett. **36**, 4368–4370 (2011).
7. S. Hu, X. Ma, D. Lu, Z. Yang, Y. Zheng, and W. Hu, "Solitons supported by complex PT-symmetric Gaussian potentials," Phys. Rev. A **84**, 043818 (2011).
8. Y. D. Chong, L. Ge, and A. D. Stone, "PT-symmetry breaking and laser-absorber modes in optical scattering systems," Phys. Rev. Lett. **106**, 093902 (2011).
9. L. Ge, Y. D. Chong, and A. D. Stone, "Conservation relations and anisotropic transmission resonances in one-dimensional PT-symmetric photonic heterostructures," Phys. Rev. A **85**, 023802 (2012).
10. Z. Lin, J. Schindler, F. M. Ellis, and T. Kottos, "Experimental observation of the dual behavior of PT-symmetric scattering," Phys. Rev. A **85**, 050101 (2012).
11. S. Hu, X. Ma, D. Lu, Y. Zheng, and W. Hu, "Defect solitons in parity-time symmetric optical lattices with nonlocal nonlinearity," Phys. Rev. A **85**, 043826 (2012).
12. B. Peng, S. K. Özdemir, F. Lei, F. Monifi, M. Gianfreda, G. L. Long, S. Fan, F. Nori, C. M. Bender, and L. Yang, "Parity-time-symmetric whispering-gallery microcavities," Nat. Phys. **10**, 394–398 (2014).
13. R. Fleury, D. Sounas, and A. Alù, "An invisible acoustic sensor based on parity-time symmetry," Nat. Commun. **6**, 5905 (2015).
14. L. Jin, X. Z. Zhang, G. Zhang, and Z. Song, "Reciprocal and unidirectional scattering of parity-time symmetric structures," Sci. Rep. **6**, 20976 (2016).
15. S. Ding and G. P. Wang, "Extraordinary reflection and transmission with direction dependent wavelength selectivity based on parity-time-symmetric multilayers," J. Appl. Phys. **117**, 023104 (2015).
16. P. Cao, X. Yang, S. Wang, Y. Huang, N. Wang, D. Deng, and C. T. Liu, "Ultrastrong graphene absorption induced by one-dimensional parity-time symmetric photonic crystal," IEEE Photon. J. **9**, 2200209 (2017).
17. Z. Z. Liu, Q. Zhang, Y. Chen, and J. J. Xiao, "General coupled-mode analysis of a geometrically symmetric waveguide array with nonuniform gain and loss," Photon. Res. **5**, 57–63 (2017).
18. C. M. Bender and S. Boettcher, "Real spectra in non-Hermitian Hamiltonians having PT symmetry," Phys. Rev. Lett. **80**, 5243–5246 (1998).
19. C. M. Bender, S. Boettcher, and P. N. Meisinger, "PT-symmetric quantum mechanics," J. Math. Phys. **40**, 2201–2229 (1999).
20. Z. Q. Zhang, C. C. Wong, K. K. Fung, Y. L. Ho, W. L. Chan, S. C. Kan, T. L. Chan, and N. Cheung, "Observation of localized electromagnetic waves in three-dimensional networks of waveguides," Phys. Rev. Lett. **81**, 5540–5543 (1998).
21. L. Dobrzynski, A. Akjouj, B. Djafari-Rouhani, J. O. Vasseur, and J. Zemmouri, "Giant gaps in photonic band structures," Phys. Rev. B **57**, R9388–R9391 (1998).
22. S. K. Cheung, T. L. Chan, Z. Q. Zhang, and C. T. Chan, "Large photonic band gaps in certain periodic and quasiperiodic networks in two and three dimensions," Phys. Rev. B **70**, 125104 (2004).
23. Z. Y. Wang and X. Yang, "Strong attenuation within the photonic band gaps of multiconnected networks," Phys. Rev. B **76**, 235104 (2007).
24. X. Xu, X. Yang, S. Wang, T. C. Liu, and D. Deng, "Sufficient condition for producing photonic band gaps in one-dimensional optical waveguide networks," Opt. Express **23**, 27576–27588 (2015).
25. X. Yang, H. Song, and T. C. Liu, "Comb-like optical transmission spectrum resulting from a four-cornered two-waveguide-connected network," Phys. Lett. A **377**, 3048–3051 (2013).
26. Y. Wang, X. Yang, J. Lu, G. Zhang, and C. T. Liu, "Comb-like optical transmission spectra generated from one-dimensional two-segment-connected two-material waveguide networks optimized by genetic algorithm," Phys. Lett. A **378**, 1200–1207 (2014).
27. J. Lu, X. Yang, G. Zhang, and L. Cai, "Large photonic band gaps and strong attenuations of two-segment-connected Peano derivative networks," Phys. Lett. A **375**, 3904–3909 (2011).
28. Q. Xiao, X. Yang, J. Lu, and C. Liu, "Huge photonic band gaps with strong attenuations resulted from quasi-one-dimensional waveguide networks composed of triangular fundamental loops," Opt. Commun. **285**, 3775–3780 (2012).
29. Z. Tang, X. Yang, J. Lu, and C. T. Liu, "Super-strong photonic localization in symmetric two-segment-connected triangular defect waveguide networks," Opt. Commun. **331**, 53–58 (2014).
30. N. Wang, X. Yang, X. Xu, Y. Huang, P. Cao, D. Deng, C. T. Liu, and X. Hu, "Strong photonic localizations generated in single-optical-waveguide ring," IEEE Photon. J. **8**, 4502513 (2016).
31. X. Hu, X. Yang, and D. Deng, "A novel approach for generating giant electronic persistent currents in symmetric defect mesoscopic-ring networks," Phys. Lett. A **381**, 1241–1247 (2017).
32. L. Feng, Y. L. Xu, W. S. Fegadolli, M. H. Lu, J. E. B. Oliveira, V. R. Almeida, Y. F. Chen, and A. Scherer, "Experimental demonstration of a unidirectional reflectionless parity-time metamaterial at optical frequencies," Nat. Mater. **12**, 108–113 (2013).
33. M. J. Dodge, "Refractive properties of magnesium fluoride," Appl. Opt. **23**, 1980–1985 (1984).
34. Y. Liu, Z. Hou, P. M. Hui, and W. Sritrakool, "Electronic transport properties of Sierpinski lattices," Phys. Rev. B **60**, 13444–13452 (1999).
35. Z. Q. Zhang and P. Sheng, "Wave localization in random networks," Phys. Rev. B **49**, 83–89 (1994).
36. S. Phang, T. M. Benson, H. Susanto, S. C. Creagh, G. Gradoni, P. D. Sewell, and A. Vukovic, *Recent Trends in Computational Photonics* (Springer, 2017).
37. Y. Choi, C. Hahn, J. W. Yoon, S. H. Song, and P. Berini, "Extremely broadband, on-chip optical nonreciprocity enabled by mimicking nonlinear anti-adiabatic quantum jumps near exceptional points," Nat. Commun. **8**, 14154 (2017).